Cite this : New Carbon Materials, 2024, 39(1): 164-172 **DOI:** 10.1016/S1872-5805(24)60832-2

Ir nanoclusters on ZIF-8-derived nitrogen-doped carbon frameworks to give a highly efficient hydrogen evolution reaction

WANG Xi-ao[1], GONG Yan-shang[1], LIU Zhi-kun[2], WU Pei-shan[3,*], ZHANG Li-xue[1], SUN Jian-kun[1,*]

(1. *College of Chemistry and Chemical Engineering*, *Collaborative Innovation Center for Hydrogen Energy Key Materials and Technologies of Shandong Province*, *Qingdao University*, *Qingdao* 266071, *China*;
2. *Wanhua Chemical Group Co., Ltd.*, *Yantai* 264000, *China*;
3. *Institute of Analysis*, *Guangdong Academy of Sciences*, *Guangdong Provincial Key Laboratory of Emergency Test for Dangerous Chemicals*, *Guangzhou* 510070, *China*)

Abstract: The precise change of the electronic structure of active metals using low-active supports is an effective way of developing high-performance electrocatalysts. The electronic interaction of the metal and support provides a flexible way of optimizing the catalytic performance. We have fabricated an efficient hydrogen evolution reaction (HER) electrocatalyst, in which Ir nanoclusters are uniformly loaded on a nitrogen-doped carbon framework (Ir@NC). The synthesis process entails immersing an annealed zeolitic imidazolate framework-8 (ZIF-8), prepared at 900 °C as a carbon source, into an $IrCl_3$ solution, followed by a calcination-reduction treatment at 400 °C under a H_2/Ar atmosphere. The three-dimensional porous structure of the nitrogen-doped carbon framework exposes more active metal sites, and the combined effect of the Ir clusters and the N-doped carbon support efficiently changes the electronic structure of Ir, optimizing the HER process. In acidic media, Ir@NC has a remarkable HER electrocatalytic activity, with an overpotential of only 23 mV at 10 mA cm^{-2}, an ultra-low Tafel slope (25.8 mV dec^{-1}) and good stability for over 24 h at 10 mA cm^{-2}. The high activity of the electrocatalyst with a simple and scalable synthesis method makes it a highly promising candidate for the industrial production of hydrogen by splitting acidic water.

Key words: Ir nanoclusters; Nitrogen-doped carbon support; Electronic interaction; Electrocatalysis; Hydrogen evolution reaction

1 Introduction

Hydrogen energy with high energy density is a clean and sustainable energy resource which can be easily transported and stored, allowing for flexibility in energy distribution[1–3]. Additionally, hydrogen fuel cells have high energy conversion efficiency and produce only water as a byproduct, minimizing environmental impact[4–5]. However, obtaining green hydrogen via water electrolysis is largely hindered by its low energy efficiency. Recently, acidic electrolyzers, generally operate at lower voltages and have higher energy efficiency than alkaline counterparts, have become interesting alternatives[6–8]. Furthermore, acidic electrolyzers also exhibit faster reaction kinetics, enabling higher current densities and overall improved performance[9]. However, one major challenge in acidic catalytic systems is the stability of the catalysts. Most of the catalysts that can be utilized in alkaline conditions, especially the non-noble metal catalysts, are severely degraded in acidic electrolytes[10–12]. This instability can lead to decreased catalytic activity and shortened catalyst lifespan[13–14]. Addressing catalyst stability is crucial for the development and commercialization of efficient and durable electrocatalytic hydrogen production in acidic conditions[15].

Despite the low abundance and high cost, precious metals like Pt, Ir and Ru are still the main electrocatalysts that are extensively utilized in acidic electrolytes[16–17]. For instance, You et al. reported Ir nanoparticles anchored cucurbit [6] uril, which exhibited

Received date: 2023-10-21; **Revised date:** 2023-11-29

Corresponding author: WU Pei-shan, Research assistant. E-mail: wupeishan@fenxi.com.cn;
SUN Jian-kun, Professor. E-mail: sunjk@qdu.edu.cn

Author introduction: WANG Xi-ao, Master student. E-mail: wangxiao_o@126.com

Supplementary data associated with this article can be found in the online version.

Homepage: http://xxtcl.sxicc.ac.cn/

slightly worse HER performance (η_{10} = 54 mV) than Pt/C in 0.5 mol L^{-1} H_2SO_4[18]. Song et al. reported that a material with Ru dispersed on CoP nanoparticles exhibits superior HER catalytic activity, with a low overpotential of 49 mV to achieve 10 mA cm^{-2} in 0.5 mol L^{-1} H_2SO_4 solution, by lowering the energy barrier of proton-coupled electron transfer[19]. Drouet et al. reported a porous Ru nanomaterial, which needed an overpotential of 83 mV to deliver 10 mA cm^{-2} in 0.5 mol L^{-1} H_2SO_4 solution, owing to the porous structure of the material[20]. Although great progress has been made in this direction, methods for regulating the electronic structure while simultaenously increasing the utilization efficiency of precious metal atoms is still challenging[21].

Nanoscaling of material dimensions plays a critical role in enhancing the specific surface area of catalysts to provide more active sites[22]. The nano-catalysts often exhibit distinct and impressive properties compared to bulk materials. In particular, the metal nanoclusters with extremely high specific surface area and a lower surface metal-metal coordination number, improve the surface-to-volume ratio as well as the atomic efficiency of catalyst[23]. However, as the size decreases, the catalysts with much higher surface energy become fragile and unstable, inducing degradation and collapse of the active components. The metal-support interaction has been considered as a promising approach to regulate the electronic structure of the active sites and simultaneously prevent side reactions that destroy their structures[24–26]. For instance, Xiao and co-workers reported an IrMo nanocluster-embedded N-rich electrocatalyst under alkaline conditions, which possesses ultrasmall bimetal nanoclusters and distinctive porous structures, enhancing the activity and stability of metal nanoclusters[27]. In addition, Zhang et al. reported a catalyst with Ir clusters loaded on Pd nanosheets, in which the charge redistribution results in an optimum hydrogen adsorption at the interface[28]. Apparently, loading precious metal nanocluster catalysts on stable supports will enable the combination of optimized electronic structure and enhanced stability in acidic electrolytes, but challenging.

Herein, we utilized annealed ZIF-8 as a carbon source to achieve uniform loading of Ir nanoclusters with an average diameter of 1.78 nm onto a three-dimensional porous N-doped carbon scaffold. This was accomplished by a simple impregnation and calcination-reduction method. The formation of strong covalent Ir-N bonds effectively suppressed the corrosion and agglomeration of Ir clusters in acidic environments. Moreover, the iridium element in Ir@NC exhibited a lower valence state compared to the Ir@C sample, which is conducive to the HER process. This is attributed to the abundant N doped in the carbon support, which regulates the electronic structure of Ir through a strong electronic effect[29]. As a result, the electrocatalyst exhibits superior HER performance than Pt/C under acidic conditions. This work demonstrates the importance of selecting appropriate catalyst supports to improve the intrinsic activity of metals and highlights the potential of N-doped carbon materials in enhancing the HER performance of Ir-based catalysts under acidic conditions.

2 Experimental section

2.1 Synthesis of NC

To prepare the ZIF-8 precursor, 2-methylimidazole (5.677 g) and hexadecyl trimethyl ammonium bromide (CTAB) (0.018 g) were dissolved in 87 mL of deionized water. Then the 13 mL of deionized water containing 0.367 g of $Zn(NO_3)_2·6H_2O$ was mixed with the above solution. The solution was stirred and aged for 6 h. Then the product was collected and dried at 60 °C. The dried ZIF-8 was subsequently annealed in a 10% H_2/Ar atmosphere at 900 °C for 2 h. This process resulted in the formation of a black nitrogen-doped carbon (NC) powder.

2.2 Synthesis of Ir@NC

To prepare Ir@NC, NC (0.025 g) and $IrCl_3·nH_2O$ (0.005 g) were dispersed in 1 mL of deionized water. Then the solution was kept at 60 °C for 6 h. The resulting product was collected, washed and dried at 60 °C under vacuum conditions. Next, the dried product was annealed at 400 °C for 4 h in a H_2/Ar at-

mosphere. After cooling down, the black colored Ir@NC powder was obtained.

For comparison, Ir@C was prepared using a similar process, but instead of NC, Ketjenblack ECP-600JD was used as the carbon support.

3 Results and discussion

The synthesis of Ir@NC sample involves a simple three-step method (Fig. 1). First, ZIF-8 was obtained by solvothermal treatment and the structure was confirmed by X-ray diffraction (XRD) patterns with the observed diffraction peaks consistent with the simulated ones (Fig. S1). Then, a porous NC skeleton was fabricated by pyrolyzing ZIF-8 at 900 °C. The diffraction peaks of ZIF-8 disappeared and 2 broad peaks at approximately 26° and 44° that belong to the graphitic carbon structure (Fig. 2a) were observed, confirming the formation of the NC skeleton[30]. Subsequently, the NC sample was immersed in an Ir^{3+} solution to obtain Ir precursor@NC. Finally, the reduction of Ir^{3+} to Ir^0 clusters was carried out under H_2/Ar conditions, resulting in the formation of Ir@NC. Notably, no diffraction peak of Ir was observed probably due to the small size.

Scanning electron microscopy (SEM) and transmission electron microscopy (TEM) were used to characterize the morphology and structure of the prepared samples. SEM image of ZIF-8 in Fig. 2b exhibits a uniform cubic shape with a size of 140 nm. After the pyrolysis treatment, the NC sample maintains its initial cubic morphology, but a reduced particle size of 75 nm due to the evaporation of In[31–32] (Fig. 2c). Upon the incorporation of Ir clusters, the size of Ir@NC is further reduced, presenting a shrunken cubic shape with a smaller size of 60 nm (Fig. 2d). TEM images of Ir@NC (Fig. 2e, f) reveal that ultra-small Ir clusters are uniformly distributed on the cubic N-doped carbon framework. This uniform dispersion can be attributed to the abundance of N atoms on the NC substrate, which act as coordinating atoms and provide nucleation sites for the formation of Ir clusters[33]. The average size of the Ir clusters is approximately 1.78 nm (Fig. 2g and Fig. S2), explaining the absence of the Ir diffraction peaks in the XRD pattern. As shown in Fig. S3, a weak diffuse ring pattern for the Ir@NC sample is found from selected-area electron diffraction (SAED) images, consistent with the results of TEM and XRD. Moreover, high-angle annular dark-field scanning TEM (HAADF-STEM) images further demonstrate the uniform distribution of Ir clusters supported on the NC substrate (Fig. 2h), and X-ray energy dispersive spectroscopy (EDS) elemental mapping images confirm the coexistence of C, N and Ir elements in the Ir@NC sample (Fig. 2i). The Ir content in Ir@NC, determined by inductively coupled plasma optical emission spectrometry (ICP-OES), was found to be 8.02%, which is in good agreement with the EDS result (Table S1). For comparison, Ir@C sample was prepared using a similar process, but with carbon black instead of ZIF-8 as the carbon source. From the XRD pattern shown in

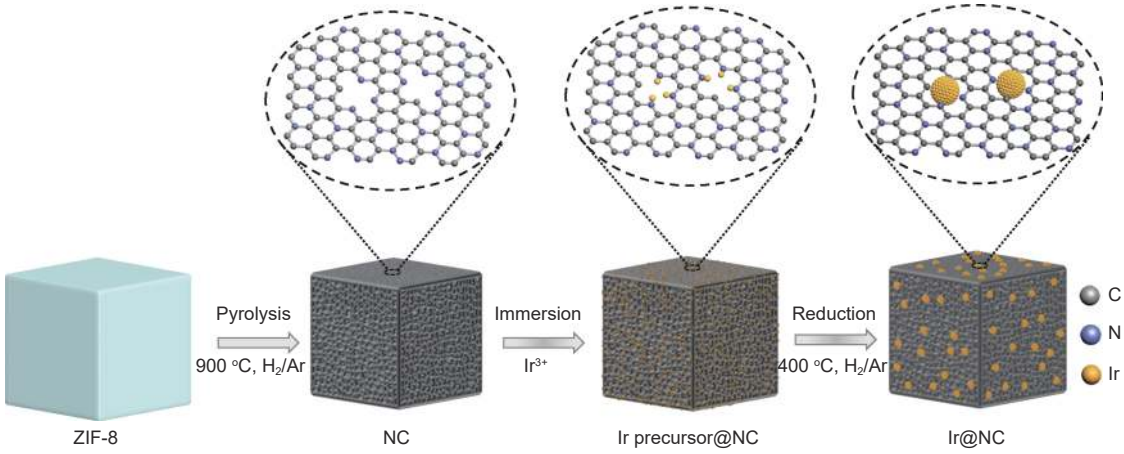

Fig. 1 Schematic illustration of the formation of Ir@NC electrocatalyst

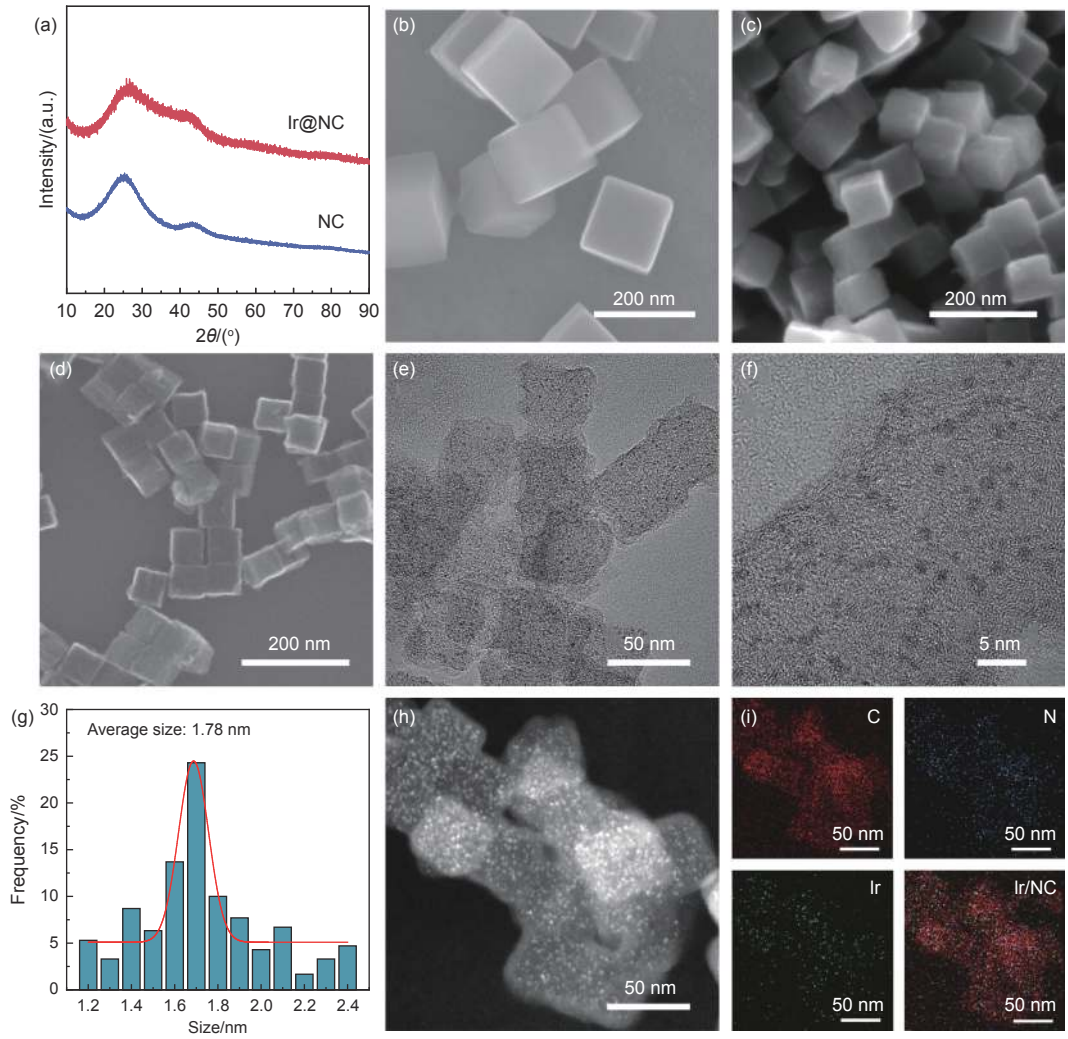

Fig. 2　(a) XRD patterns of NC and Ir@NC sample. SEM images of (b) ZIF-8, (c) NC and (d) Ir@NC. (e-f) HRTEM images of Ir@NC. (g) Size distribution of Ir nanoclusters. (h) HAADF-STEM and (i) the corresponding EDS elemental mapping images of Ir@NC

Fig. S4, no diffraction peaks corresponding to Ir were detected in the Ir@C sample. Instead, only two broad peaks attributed to the graphitic carbon structure were observed, which is similar to the Ir@NC sample.

The specific surface area and pore structure of NC and Ir@NC were determined by nitrogen adsorption/desorption analysis. The Brunauer-Emmett-Teller (BET) surface area of NC and Ir@NC was calculated to be 1 060 and 1 163 $m^2\ g^{-1}$, respectively (Fig. 3a and Table S2). The higher surface area of Ir@NC can be due to the incorporation of Ir clusters. Both the NC and Ir@NC samples exhibit a hierarchical pore structure with micropores and mesopores, as indicated by the hysteresis curves and hysteresis loop, which is verified by the pore size distribution curves (Fig. 3b). This presence of micropores facilitates the ion diffusion in the electrolyte, while the mesoporous structure enhances the mass transport of active species and enables the exposure of more active sites. Therefore, the synergistic effect of pore structure promotes electrochemical reaction kinetics[34].

The chemical composition and valence states of Ir@NC, NC and Ir@C samples were examined using X-ray photoelectron spectroscopy (XPS). The existence of the corresponding elements is confirmed by the XPS survey spectra of each sample (Fig. 4a and Fig. S5). The weak peak of Zn 2p appears in both Ir@NC and NC samples due to the incomplete removal of Zn from ZIF-8. The residual Zn does not significantly contribute to the catalytic activity[26], as will be further verified by the following electrochemical characterization. The O element detected in the spec-

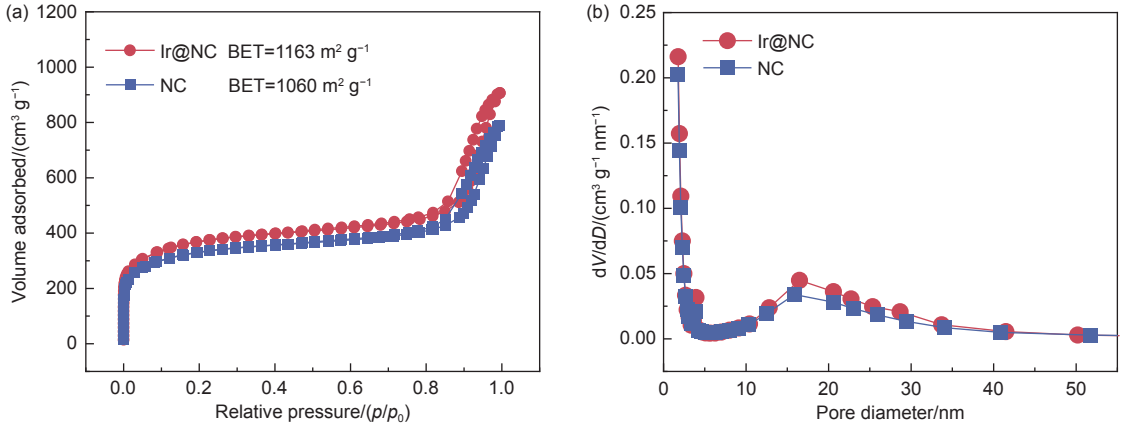

Fig. 3 (a) N_2 adsorption-desorption isotherms and corresponding (b) pore diameter distribution curves of NC and Ir@NC

tra originates from inevitable surface oxidation when exposed to air. In the C 1s spectra (Fig. 4b), the fitted peaks located at 284.8 and 286.3 eV belong to C—C and C—N coordination, respectively.

In the N 1s spectra of NC and Ir@NC samples (Fig. 4c), the signal can be well fitted with 5 peaks corresponding to pyridinic nitrogen (398.4 eV), metal—nitrogen bond (399.7 eV), pyrrolic nitrogen (400.8 eV), graphitic nitrogen (401.9 eV), and oxidic nitrogen (404.1 eV) species, respectively. The presence of metal—nitrogen bond in the NC sample mainly originates from residual Zn, while Ir@NC possesses both Zn—N and Ir—N bonds. Apart from pyridinic N and metal—N, the other nitrogen species in both samples have nearly the same content. The pyridinic N and metal—N account for 35% and 9% of the total N atoms in the NC sample, while in Ir@NC, these 2 species account for 30% and 14%, respect-

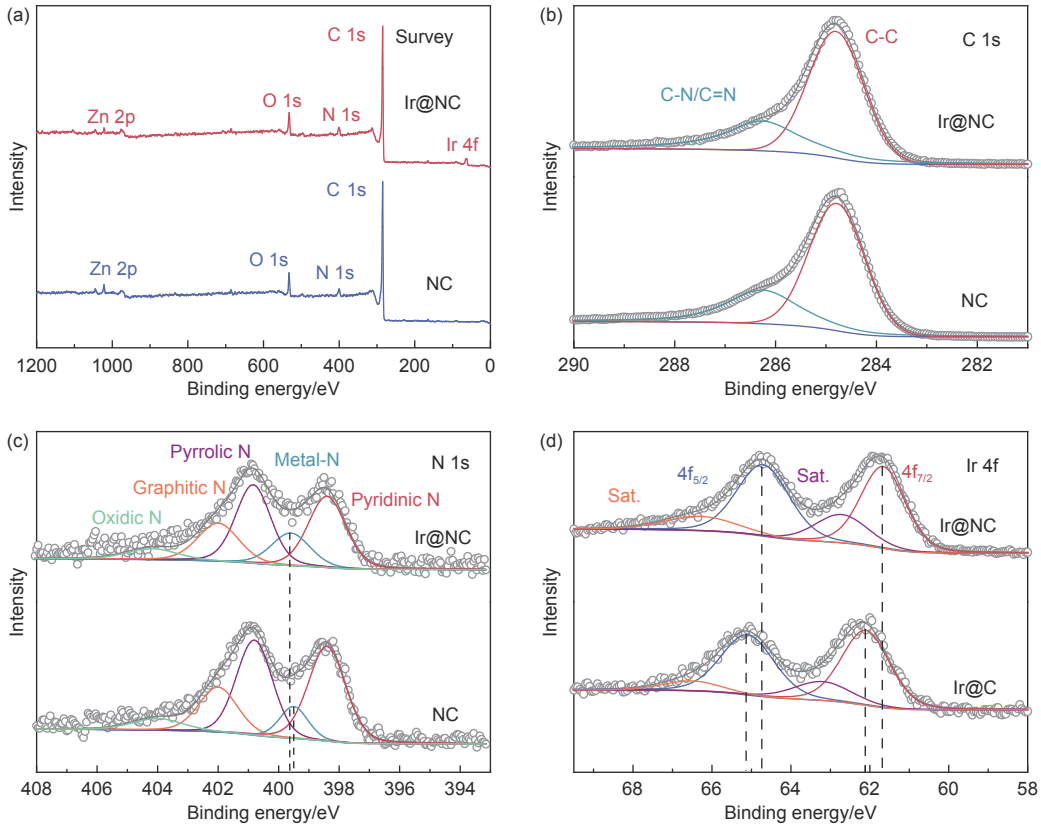

Fig. 4 XPS spectra of NC and Ir@NC. (a) Survey scan spectra of NC and Ir@NC. High-resolution spectra of (b) C 1s and (c) N 1s for Ir@NC and NC. (d) High-resolution spectra of Ir 4f for Ir@NC and Ir@C

ively. This difference indicates that a portion of pyridinic N was converted into metal-nitrogen bonds owing to the formation of Ir—N bonds with the incorporation of Ir clusters. The electron-donating properties of pyridinic N enable it to serve as metal-coordination sites to immobilize the Ir atoms[33–34]. Additionally, the peak of metal—N in Ir@NC was shifted to a higher binding energy, suggesting the significant electronic interaction between pyridinic N and Ir atoms. In the Ir 4f spectra (Fig. 4d), doublet peaks of Ir $4f_{7/2}$ and Ir $4f_{5/2}$ with 2 satellite peaks at 62.9 and 66.2 eV were observed. Compared to Ir@C, the binding energies of Ir $4f_{7/2}$ and Ir $4f_{5/2}$ in Ir@NC sample are negatively shifted from 62.1 and 65.1 eV to 61.7 and 64.7 eV, manifesting the significant interaction between Ir and N, consistent with the results of the N 1s. The corresponding data and valence states of C 1s, N 1s and Ir 4f in XPS spectra have been listed in Table S3-5. The synergistic effect between Ir clusters and NC support allows to effectively regulate electronic structure of Ir and optimize electrocatalytic HER process[35–39].

The catalytic properties of different samples were evaluated in 0.5 mol L^{-1} H_2SO_4 and all linear sweep voltammetry (LSV) curves were corrected with 85% IR to eliminate the effect of internal resistance. Notably, the immersion concentration of Ir salt solution plays a crucial role in determining the HER activity due to the different loading amounts at different concentrations, and the optimized performance was obtained at 5 mmol L^{-1} (Fig. S6). Promisingly, Ir@NC exhibited remarkable HER catalytic activity with an ultra-low overpotential of 23 mV to deliver 10 mA cm^{-2} (η_{10} = 23 mV) in acidic solution, better than the original NC with negligible activity, Ir@C (η_{10} = 37 mV), and even the commercial Pt/C (η_{10} = 28 mV) (Fig. 5b). Notably, Ir@NC outperforms the control sample, especially the sample of Ir@C, even more at higher current densities, highlighting the pivotal role of the electronic interaction between Ir and N in promoting the HER activity. Additionally, Ir@NC possesses a higher electrochemically active surface area (ECSA) of 141 m^2 g^{-1} than commercial Pt/C (30.7 m^2 g^{-1}) (Fig. S7), attributed to the well dispersed Ir nanoclusters enabled by the pyridinic N. Promisingly, the HER activity of Ir@NC outperforms most of the recently reported typical Ir-based electrocatalysts[6,9–10,18,29,33–34,40–44] (Fig. 5d). The data comparing various performance metrics, including overpo-

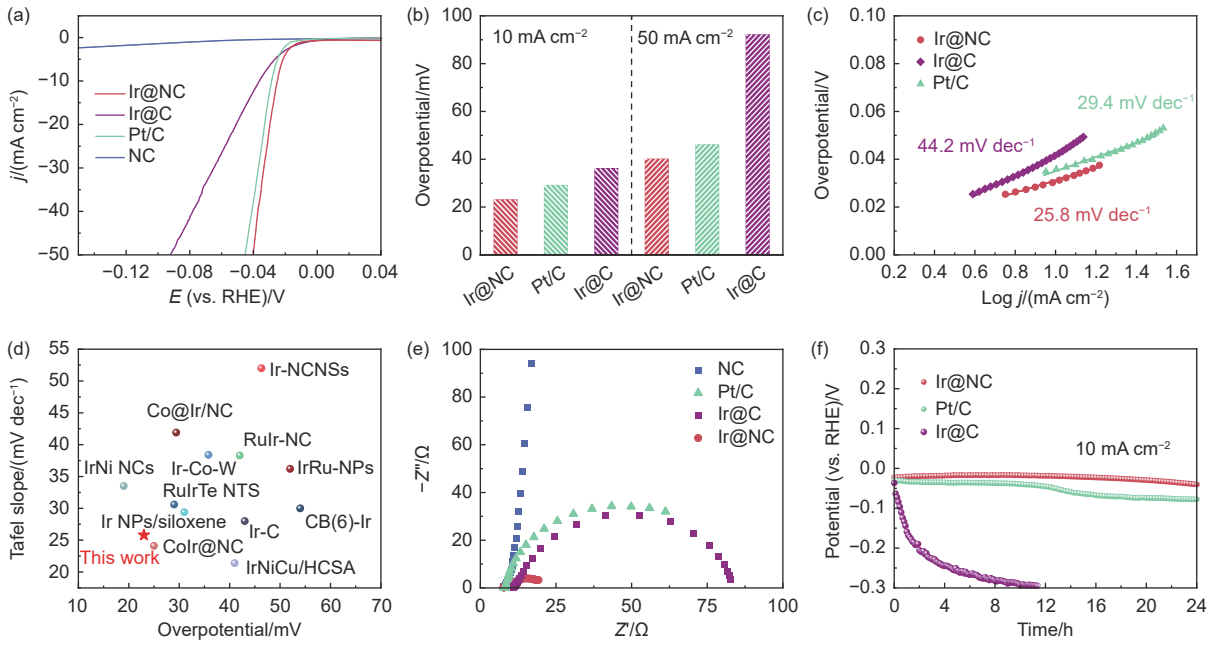

Fig. 5　HER catalytic performance of different electrocatalysts in 0.5 mol L^{-1} H_2SO_4. (a) LSV polarization curves of HER. (b) Overpotentials of different catalyst to achieve 10 and 50 mA cm^{-2}. (c) Corresponding Tafel slope. (d) Comparison of the overpotential at 10 mA cm^{-2} and Tafel slope of Ir@NC with the recently reported Ir-based HER catalysts in 0.5 mol L^{-1} H_2SO_4. (e) Nyquist plots. (f) Chronopotentiometric curves of Ir@NC, Ir@C and Pt/C at 10 mA cm^{-2} without IR correction

tential and Tafel slope, have been list in Table S6. Furthermore, the Tafel slope, reflecting the kinetics of the HER, is only 25.8 mV dec^{-1} for Ir@NC (Fig. 5c), indicating the Volmer-Tafel mechanism and substantially lower than Ir@C (44.2 mV dec^{-1}), even Pt/C (29.4 mV dec^{-1}). To further investigate the charge transfer and reaction kinetics of the HER process, electrochemical impedance spectroscopy (EIS) was performed. In Fig. 5e, all the Nyquist curves of different samples display a near-semicircle shape and the sample of Ir@NC exhibited the smallest diameter of the semicircle, indicating the lowest charge transfer impedance. These findings indicate that the loading of Ir on the NC support, particularly the electronic structure modification of Ir through metal-support interaction (as verified by XPS results), can expedite the charge and electron transfer process, thereby contributing to the significantly enhanced HER performance[37–38].

Ir@NC exhibits good stability at 10 mA cm^{-2} under acidic conditions for more than 24 h (Fig. 5f), apparently better than the commercial Pt/C sample and Ir@C. Additionally, the structure of the NC and the cubic morphology of the Ir@NC sample were well preserved after the stability test (Fig. S8a and S8b). More importantly, Ir nanoclusters were still well-distributed on the NC framework without any significant agglomeration and dissolution (Fig. S8c). The average size of Ir clusters after the stability test is about 1.72 nm, which is close to the original size of 1.78 nm (Fig. S8d). These results indicate that the metal-support electron interactions between the Ir clusters and the NC support inhibit the aggregation and dissolution of the Ir clusters, unambiguously contributing to the good stability of Ir@NC during HER under acidic conditions.

4 Conclusion

In conclusion, our study demonstrates the successful synthesis of uniformly dispersed ultra-small Ir nanoclusters on the porous nitrogen-doped carbon derived from ZIF-8. These Ir@NC catalysts exhibit remarkable electrocatalytic activity for HER in acidic electrolytes. With a low overpotential of only 23 mV, Ir@NC achieves 10 mA cm^{-2}, showcasing its high efficiency. The Ir nanoclusters are uniformly dispersed thanks to the rich porous structure of the N-doped carbon support. Furthermore, the existence of pyridinic N on the surface of the NC support plays a crucial role in immobilizing the Ir nanoclusters and establishing strong electron interactions between the support and the Ir clusters. This synergistic effect enhances the overall catalytic performance of Ir@NC. Additionally, the Ir@NC catalyst exhibits excellent electrochemical and structural stability, thanks to the coupling effect between the Ir and pyridinic N atoms. The facile synthesis method of Ir@NC further enhances its potential for widespread use in commercial proton exchange membrane electrolysis. These findings highlight the significance of precisely modulating the electronic structure using low-active supports in the design of high-performance electrocatalysts for efficient hydrogen production.

Acknowledgements

This research was funded by the China Postdoctoral Science Foundation (2020M671990) and the Qingdao Applied Fundamental Research Project.

References

[1] Zhang L H, Shi Y, Wang Y, et al. Nanocarbon catalysts: Recent understanding regarding the active sites[J]. Advanced Science, 2020, 7: 1902126.

[2] Wu Y Z, Huang Y, Jiang L W, et al. Modulating the electronic structure of CoS_2 by Sn doping boosting urea oxidation for efficient alkaline hydrogen production[J]. Journal of Colloid and Interface Science, 2023, 642: 574-583.

[3] Yin Z H, Huang Y, Jiang L W, et al. Revealing the In situ evolution of tetrahedral $NiMoO_4$ micropillar array for energy-efficient alkaline hydrogen production assisted by urea electrolysis[J]. Small Structures, 2023, 4: 2300028.

[4] Sun J, Xu W, Lv C, et al. Co/MoN hetero-interface nanoflake array with enhanced water dissociation capability achieves the Pt-like hydrogen evolution catalytic performance[J]. Applied Catalysis B:Environmental, 2021, 286: 119882.

[5] Yi P, Song Y, Li C, et al. Heterostructured Mn-doped NiS_x/NiO/Ni_3N nanoplate arrays as bifunctional electrocatalysts for energy-saving hydrogen production and urea degradation[J]. Applied Surface Science, 2023, 619: 156789.

[6] Zhang J, Chen Z, Liu C, et al. Hierarchical iridium-based multimetallic alloy with double-core-shell architecture for efficient overall water splitting[J]. Science China Materials, 2019, 63(2): 249-257.

[7] Reier T, Pawolek Z, Cherevko S, et al. Molecular insight in structure and activity of highly efficient, low-Ir Ir-Ni oxide catalysts for electrochemical water splitting (OER)[J]. Journal of the American Chemical Society, 2015, 137(40): 13031-13040.

[8] Wang C, Zhai P, Xia M, et al. Engineering lattice oxygen activation of iridium clusters stabilized on amorphous bimetal borides array for oxygen evolution reaction[J]. Angewandte Chemie International Edition, 2021, 60(52): 27126-27134.

[9] Kim M, Kang H, Hwang E, et al. Facile colloidal synthesis of transition metal (Co, Fe and Ni)-added Ir-W NPs for HER in acidic electrolyte[J]. Applied Surface Science, 2023, 612: 155862.

[10] Liu M, Liu S, Mao Q, et al. Ultrafine ruthenium–iridium–tellurium nanotubes for boosting overall water splitting in acidic media[J]. Journal of Materials Chemistry A, 2022, 10(4): 2021-2026.

[11] Liu Z X, Wang X L, Hu A P, et al. 3D Se-doped NiCoP nanoarrays on carbon cloth for efficient alkaline hydrogen evolution[J]. Journal of Central South University, 2021, 28(8): 2345-2359.

[12] Li C, Yi P, Sun J, et al. Robust self-supported SnO_2-Mn_2O_3@CC electrode for efficient electrochemical degradation of cationic blue X-GRRL dye[J]. Molecules, 2023, 28: 3957.

[13] Chatti M, Gardiner J L, Fournier M, et al. Intrinsically stable in situ generated electrocatalyst for long-term oxidation of acidic water at up to 80 °C[J]. Nature Catalysis, 2019, 2(5): 457-465.

[14] Cheng A, Zhao J, Wang X A, et al. Hybrid 1D/3D-structured perovskite as a highly selective and stable sensor for NO_2 detection at room temperature[J]. Molecules, 2023, 28: 2615.

[15] Huang Y, Jiang L W, Liu H, et al. Electronic structure regulation and polysulfide bonding of Co-doped $(Ni, Fe)_{1+x}S$ enable highly efficient and stable electrocatalytic overall water splitting[J]. Chemical Engineering Journal, 2022, 441: 136121.

[16] Yin S H, Yang S L, Li G, et al. Seizing gaseous Fe^{2+} to densify O_2-accessible Fe –N_4 sites for high-performance proton exchange membrane fuel cells[J]. Energy & Environmental Science, 2022, 15(7): 3033-3040.

[17] Meng C, He W D, Tan H, et al. A eutectic electrolyte for an ultralong-lived Zn//V_2O_5 cell: an in situ generated gradient solid-electrolyte interphase[J]. Energy & Environmental Science, 2023, 16(8): 3587-3599.

[18] You H, Wu D, Chen Z N, et al. Highly active and stable water splitting in acidic media using a bifunctional iridium/cucurbit[6]uril catalyst[J]. ACS Energy Letters, 2019, 4(6): 1301-1307.

[19] Song H, Wu M, Tang Z, et al. Single atom ruthenium-doped CoP/CDs nanosheets via splicing of carbon-dots for robust hydrogen production[J]. Angewandte Chemie International Edition, 2021, 60: 7234-7244.

[20] Drouet S, Creus J, Colliere V, et al. A porous Ru nanomaterial as an efficient electrocatalyst for the hydrogen evolution reaction under acidic and neutral conditions[J]. Chemical Communications, 2017, 53(85): 11713-11716.

[21] Zhang Y, Huang Y, Zhu S S, et al. Covalent S-O bonding enables enhanced photoelectrochemical performance of Cu_2S/Fe_2O_3 heterojunction for water splitting[J]. Small, 2021, 17: 2100320.

[22] Ding J, Yang H, Zhang S, et al. Advances in the electrocatalytic hydrogen evolution reaction by metal nanoclusters-based materials[J]. Small, 2022, 18: 2204524.

[23] Dong C, Li Y, Cheng D, et al. Supported metal clusters: Fabrication and application in heterogeneous catalysis[J]. ACS Catalysis, 2020, 10(19): 11011-11045.

[24] Zhang X, Sa R, Yang S, et al. A non-carbon catalyst support upgrades the intrinsic activity of ruthenium for hydrogen evolution electrocatalysis via strong interfacial electronic effects[J]. Nano Energy, 2020, 75: 104981.

[25] Xue S G, Tang L, Tang T, et al. Identifying the active sites in C-N codoped TiO_2 electrode for electrocatalytic water oxidation to produce H_2O_2[J]. Journal of Central South University, 2022, 29(9): 3016-3029.

[26] Wang Q, Xu C Q, Liu W, et al. Coordination engineering of iridium nanocluster bifunctional electrocatalyst for highly efficient and pH-universal overall water splitting[J]. Nature Communications, 2019, 10: 4875.

[27] Xiao X, Li Z, Xiong Y, et al. IrMo nanocluster-doped porous carbon electrocatalysts derived from cucurbit[6]uril boost efficient alkaline hydrogen evolution[J]. Journal of the American Chemical Society, 2023, 145(30): 16548-16556.

[28] Shi J, Kao C W, Lan J, et al. Nanoporous PdIr alloy for high-efficiency and durable water splitting in acidic media[J]. Journal of Materials Chemistry A, 2023, 11(21): 11526-11533.

[29] Chen W, Xie Y, Gao X, et al. Simultaneous optimization of CoIr alloy nanoparticles and 2D graphitic-N doped carbon support in CoIr@CN by Ir doping for enhanced oxygen and hydrogen evolution reactions[J]. Journal of Materials Chemistry A, 2022, 10(29): 15543-15553.

[30] Wang M, Zheng X, Qin D, et al. Atomically dispersed CoN_3C_1-TeN_1C_3 diatomic sites anchored in N-doped carbon as efficient bifunctional catalyst for synergistic electrocatalytic hydrogen evolution and oxygen reduction[J]. Small, 2022, 18: 2201974.

[31] Wei S, Li A, Liu J C, et al. Direct observation of noble metal nanoparticles transforming to thermally stable single atoms[J]. Nature Nanotechnol, 2018, 13: 856-861.

[32] Liang Q, Li Q, Xie L, et al. Superassembly of surface-enriched Ru nanoclusters from trapping-bonding strategy for efficient hydrogen evolution[J]. ACS Nano, 2022, 16: 7993-8004.

[33] Wu X, Wang Z, Chen K, et al. Unravelling the role of strong metal-support interactions in boosting the activity toward hydrogen evolution reaction on Ir nanoparticle/N-doped carbon nanosheet catalysts[J]. ACS Applied Materials & Interfaces, 2021, 13: 22448-22456.

[34] Li D, Zong Z, Tang Z, et al. Total water splitting catalyzed by Co@Ir core –shell nanoparticles encapsulated in nitrogen-doped porous carbon derived from metal –organic frameworks[J]. ACS

Sustainable Chemistry & Engineering, 2018, 6(4): 5105-5114.

[35] Mao Y, Chen J, Wang H, et al. Catalyst screening: Refinement of the origin of the volcano curve and its implication in heterogeneous catalysis[J]. Chinese Journal of Catalysis, 2015, 36(9): 1596-1605.

[36] Chen H, Ai X, Liu W, et al. Promoting subordinate, efficient ruthenium sites with interstitial silicon for Pt - like electrocatalytic activity[J]. Angewandte Chemie International Edition, 2019, 58: 11409-11413.

[37] Li F, Han G F, Noh H J, et al. Balancing hydrogen adsorption/desorption by orbital modulation for efficient hydrogen evolution catalysis[J]. Nature Communications, 2019, 10: 4060.

[38] Zhao Y, Watanabe K, Hashimoto K. Self-supporting oxygen reduction electrocatalysts made from a nitrogen-rich network polymer[J]. Journal of the American Chemical Society, 2012, 134(48): 19528-19531.

[39] Artyushkova K, Kiefer B, Halevi B, et al. Density functional theory calculations of XPS binding energy shift for nitrogen-containing graphene-like structures[J]. Chemical Communications, 2013, 49(25): 2539-2541.

[40] Joo J, Jin H, Oh A, et al. An IrRu alloy nanocactus on $Cu_{2-x}S$@IrS_y as a highly efficient bifunctional electrocatalyst toward overall water splitting in acidic electrolytes[J]. Journal of Materials Chemistry A, 2018, 6(33): 16130-16138.

[41] Wu D, Kusada K, Yoshioka S, et al. Efficient overall water splitting in acid with anisotropic metal nanosheets[J]. Nature Communications, 2021, 12(1): 1145.

[42] Pi Y, Shao Q, Wang P, et al. General formation of monodisperse IrM (M = Ni, Co, Fe) bimetallic nanoclusters as bifunctional electrocatalysts for acidic overall water splitting[J]. Advanced Functional Materials, 2017, 27: 1700886.

[43] Peng Y, Liu Q, Lu B, et al. Organically capped iridium nanoparticles as high-performance bifunctional electrocatalysts for full water splitting in both acidic and alkaline media: Impacts of metal –ligand interfacial interactions[J]. ACS Catalysis, 2021, 11(3): 1179-1188.

[44] Dai Q, Meng Q, Du C, et al. Spontaneous deposition of Ir nanoparticles on 2D siloxene as a high-performance HER electrocatalyst with ultra-low Ir loading[J]. Chemical Communications, 2020, 56(35): 4824-4827.

Ir 纳米团簇负载于 ZIF-8 衍生的氮掺杂炭框架用于高效析氢反应

王希澳[1]， 公衍尚[1]， 刘之坤[2]， 巫培山[3,*]， 张立学[1]， 孙建坤[1,*]

（1. 青岛大学 化学化工学院，山东省氢能关键材料与技术协同创新中心，山东 青岛 266071；
2. 万华化学集团股份有限公司，山东 烟台 264000；
3. 广东省科学院测试分析研究所，广东省化学测量与应急检测技术重点实验室，广东 广州 510070）

摘 要： 利用低活性载体精确调控活性金属的电子结构是开发高性能电催化剂的有效途径，金属与载体之间高度灵活的电子相互作用可优化催化性能。在此，将 Ir 纳米团簇（Ir@NC）均匀地负载在氮掺杂炭框架上，制备了一种高效的析氢反应（HER）电催化剂。合成过程是将在 900 °C 下退火制备的沸石咪唑盐框架-8（ZIF-8）作为碳源浸入 $IrCl_3$ 溶液中，然后在 400 °C 的 H_2/Ar 气氛下进行煅烧还原处理。氮掺杂炭框架的三维多孔结构暴露了更多的活性金属位点，Ir 簇和氮掺杂炭载体之间的协同效应有效地调节了 Ir 的电子结构，优化了 HER 过程。在酸性介质中，Ir@NC 表现出显著的 HER 电催化活性：在 10 mA cm^{-2} 的条件下，过电位仅为 23 mV，具有超低的 Tafel 斜率（25.8 mV dec^{-1}），且在 10 mA cm^{-2} 的条件下可稳定运行 24 h 以上。制备的电催化剂具有高活性、合成路线简便、可规模化制备等优点，有望成为一种极有前途的候选催化剂用于酸性水裂解进行工业制氢。

关键词： 铱纳米团簇；氮掺杂炭载体；电子相互作用；电催化；析氢反应

中图分类号： TQ127.1$^+$1 **文献标识码：** A

基金项目： 中国博士后科学基金 (2020M671990)；青岛市应用基础研究项目.

通讯作者： 巫培山，助理研究员. E-mail: wupeishan@fenxi.com.cn；
孙建坤，教授. E-mail: sunjk@qdu.edu.cn

作者简介： 王希澳，硕士研究生. E-mai: wangxiao_o@126.com